Human Identification Using Finger and Iris Images

M.Bhavani[#1], Mrs.Shoba Rani[#2]

(1)M.Tech student in Computer Science and Engineering
(2) Assistant Professor in Computer Science and Engineering
Dr.MGR Educational and Research Institute, Chennai, TamilNadu, INDIA

***Abstract*— Biometric system has been actively emerging in various industries for the past few years, and it is continuing to roll to provide higher security features for access control system. In the recent years, hand based biometrics is extensively used for personal recognition. In this paper a new combined biometric system based on texture of the hand knuckles, namely Finger-Knuckle-Print (FKP) and IRIS, is proposed. To extract the image local texture information and represent the FKPs features, by Linear Discriminate Analysis (LDA) and IRIS by the 2D Block based Gabor method, is employed. Finally, performance of all finger/iris types is determined individually and a min rule fusion is applied to develop a combined authentication system. Experimental results show that LDA the best performance for identifying FKPs and Gabor is the best performance for IRIS and it is able to provide an excellent recognition rate and provide more security.**

***Keywords*— Finger Knuckle Print, IRIS, LDA, Gabor, Recognition.**

I. INTRODUCTION

Biometrics is the science of identifying a person using one's physiological or characteristics. Biometric based personal authentication is an effective method for automatically recognizing a person's identity. Human physiological and/or behavioural characteristic can be used as a biometric trait when it satisfies the requirements like ubiquity, peculiarity, stability and collectability. However, in a practical combined biometric system, one needs to consider some other issues too like efficacy, acceptableness and circumvention.

Keeping all these requirements in mind, biometric traits like fingerprints, hand veins, handwritten signatures, retinal patterns, ear patterns, electrocardiogram etc. are used extensively in areas which require security access. Among various kinds of biometric identifiers, hand-based biometrics has been attracting considerable attention over recent years due to its ease in accession. Biometric traits like fingerprint, palm print, hand geometry and hand vein and iris have been proposed and well investigated in the literature.

Recently, it has been noticed that the texture in the outer finger surface, also known as the dorsum of hand, has the potential to do personal authentication. The texture pattern produced by bending the finger knuckle of a person is highly unique and thus can serve as a distinct biometric trait. The user acceptance for the outer finger surface imaging can be very high as, unlike popular fingerprints, there is no stigma of criminal investigation associated with finger knuckle surface imaging. The peg-free imaging of the finger knuckle surface is highly convenient to users and offers very high potential for reliable personal identification and authentication. The appearance based approach investigated in for the finger knuckle identification cannot exploit line based features and therefore achieves moderate performance. The finger knuckle surface is highly rich in lines and creases, which are rather curved but highly unique for individuals.

Compared to fingerprint, iris is protected from the external environment behind the cornea and the eyelid, polar region extraction has no subject to deleterious effects of aging, the small-scale radial features of the iris remain are stable and fixed throughout life.

II. RELATED WORK

A brief survey of the related work in the area of identification and authentication using finger knuckle and iris surface is presented in this section. The image pattern formation from the finger knuckle bending is highly unique and makes this surface a distinct biometric identifier. The finger geometry features can be acquired from the same image, at the same time and integrated to improve the performance of the system.

Iris recognition is one of the most important biometric technologies. Due to its accurate and reliable advantages, this method is becoming the trend of personal authentication technologies. Iris localization is the integral part of iris recognition, which calculates the positions of iris boundaries, and extracts the iris region from other parts of the captured eye image in iris recognition. our classical iris localization methods is shown below.

$$\max(r, x_0, y_0)\left|G_\sigma(r) * \frac{\partial}{\partial r} \oint_{r,x_0,y_0} \frac{I(x,y)}{2\pi r} ds\right| \qquad (1)$$

Where * denotes convolution and $G_\clubsuit(r)$ is a smoothing function. The method searches on the three dimension space (r, x_0, y_0), so it takes a long time to complete the localization.

And the other is Gabor method; Gabor method presents a robust, real-time algorithm for localizing the iris and pupil boundaries of an eye in a close-up image. It uses a multi-resolution approach to detect the boundary

contours of interest quickly and reliably, even in cases of very low contrast, specular reflections and oblique views. The Wilds' method localizes the outer boundary of the iris first and then localizes the inner boundary inside the outer one. The method has a high computational cost, since it searches among all the potential candidates.

III. ARCHITECTURE AND MODELING

Having the database of FKP images of all the people in an organization consumes more space and the complexity of the system will increase. So, we suggest having user identification number (UID) for each person. The FKP image features like number of peaks in the Gabor Wavelet graph and the successive distances between those peaks are stored in the database corresponding to particular UID. During authentication, the person has to provide the UID and his FKP image is captured. If the features of new image match with the corresponding features in the database, the person can be authenticated.

A. *FKP Image Acquisition*

A specially get FKP image acquisition databases can be used to take FKP image from a subject. The proposed algorithm is simulated on PolyU FKP Database.

B. *Pre-processing*

The captured image is converted from RGB to gray-scale format. Then the region of interest (ROI) is extracted from FKP image as explained in . The original FKP image and ROI for one of the subjects is shown in Figure 1(a) and 1(b) respectively. The edges are detected by looking for local maxima of the gradient of image. The gradient is calculated using the derivative of a Gaussian filter. The gradient of an image *f(x, y)* at location *(x, y)* is defined as the vector –

$$\nabla f = \begin{bmatrix} G_x \\ G_y \end{bmatrix} = \begin{bmatrix} \frac{\partial f}{\partial x} \\ \frac{\partial f}{\partial y} \end{bmatrix} \quad (2)$$

An important quantity in edge detection is the magnitude of this vector, denoted ∇f, where

$$\nabla f = mag(\nabla f) = \left[G_x^2 + G_y^2 \right]^{\frac{1}{2}} \quad (3)$$

The method uses two thresholds to detect strong and weak edges, and includes the weak edges in the output only if they are connected to strong edges. Fig. 2 shows the image after edge detection. The algorithm for detecting the edges of ROI image is given in Table I. Then order-statistics filters are used, whose response is based on ordering (ranking) the pixels contained in the image area encompassed by the filter. The response of the filter at any point is then determined by the ranking result. The current algorithm uses Median filter, the best-known order-statistics filter, which is given as –

$$\hat{f}(x, y) = median_{(s, t) \in S_{xy}} \{ g(s,t) \} \quad (4)$$

Here, S_{xy} represent the set of coordinates in a rectangular sub-image window of size m x n centered at point (x, y). Morphological opening is applied to smoothen the contour of the edges and to eliminate thin protrusions. Then the image is dilated to expand the obtained edges. Fig. 2 shows the image after dilation.

C. *Feature Extraction*

The features extracted must be non-trivial and must not vary for a given person over time. We apply Gabor Wavelet transform on the image obtained after pre-processing. A Gabor wavelet is a complex planar wave restricted by a two-dimensional Gaussian envelope. Gabor wavelet contains two components viz. real and imaginary. Aside from scale and orientation, the only thing that can make two Gabor wavelets differ is the ratio between wavelength and the width of the Gaussian envelope. Every Gabor wavelet has a certain wavelength and orientation, and can be convolved with an image to estimate the magnitude of local frequencies of that approximate wavelength and orientation in the image.

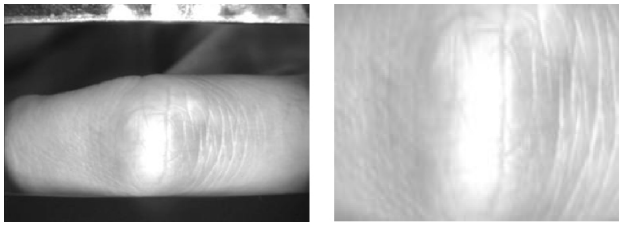

(a) Original FKP Image (b) Extracted ROI

Fig. 1 Test Image 1

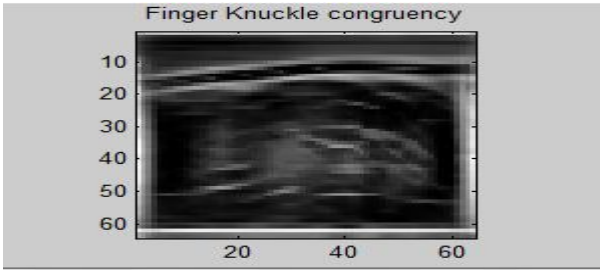

Fig. 2 Phase Congruency and LDA for Test Image1

TABLE I
EDGE DETECTION ALGORITHM

1. The input image is smoothed using a Gaussian filter with a specified standard deviation σ, to reduce noise.

2. The local gradient, $g(x, y) = [G_x^2 + G_y^2]^{12}$, and edge point

$$\frac{G_x}{G_y}$$

Here, G_x and G_y are first derivatives. An edge point is defined to be a point whose strength is locally maximum in the direction of the gradient.

3. The edge points determined in Step 2 give rise to ridges in the gradient magnitude image. The algorithm then tracks along the top of these ridges and sets to zero all pixels that are not actually on the ridge top so as to give a thin line in the output, a process known as non-maximal suppression. The ridge pixels are then thresholded using two thresholds T1 and T2, with T1 < T2. Ridge pixels with values greater than T2 are said to be strong edge pixels. Ridge pixels with values between T1 and T2 are said to be weak edge pixels.

4. Finally, the algorithm performs edge linking by incorporating the weak pixels with that are 8-connected to the strong pixels.

The 2D Gabor wavelet is separable, that is, it can be represented as a convolution of two orthogonal 1D Components. These components are: a Gaussian *g(x)*, and a wavelet *w(x)* (a complex wave enveloped by a Gaussian), defined respectively by –

$$\frac{1}{\sqrt{2\pi\sigma^2}} \qquad \frac{x^2}{2\sigma^2} \qquad (5)$$

and

$$w(x) = g(x)e^{j\omega x} \qquad (6)$$

where $j = \sqrt{-1}$ and ω is the frequency of the wavelet. These functions describe the separable components of a Gabor filter kernel. It follows that convolution of a Gabor kernel with an image can be calculated separately. For example, a horizontally aligned *n* x *n* Gabor kernel ***K*** can be written as –

$$\boldsymbol{K} = g * w \qquad (7)$$

where *g* and *w* are *nx1* vectors whose elements are defined by regularly sampling *g(x)* and *w(x)* across intervals centered at *x = 0*. The convolution of ***K*** with an image ***I*** is then

$$I * K = I * (g * w^T) = (I * g) * w^T \qquad (8)$$

Note that *w* is complex, so the ***I *g*** convolution is performed first in order that only the last convolution require complex arithmetic.

By applying Gabor wavelet on a pre-processed FKP image, we will get Gabor image as shown in Figure 3.

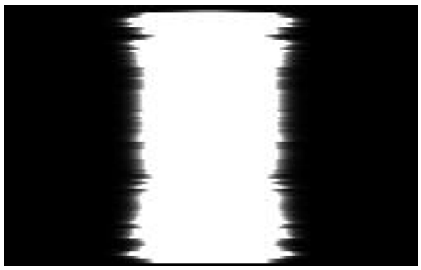

Fig. 3 Gabor Image obtained for Test Image1

Against each row of Gabor Wavelet matrix containing width of Gaussian envelope, the wavelength is plotted as a graph and the peak values are marked. Peak values are nothing but the local maxima. A real -valued function *f (x)* is said to have a local maximum point at the point x^*, if there exists some ε > 0 such that –

$$f(x^*) \geq f(x) \text{ where, } |x - x^*| < \Sigma \qquad (9)$$

The value of the function at this point is called maximum of that function. In other words, each value in the graph is compared to its neighbouring values, and if it is larger than both of its neighbours, it is a local peak. Identified peak points of a Gabor Wavelet graph for the subject are plotted as shown in Figure 3. The number of such peak-points is stored in the database as a feature. The coordinate positions of all the peaks are stored as another feature-set.

D. Feature Matching

The next step is to compute the parameters needed for decision making towards authentication. The number of peak-points in a Gabor Wavelet graph retrieved from the database and that of input subject are compared. The slight displacement of a finger during image acquisition may lead to possible difference in number of peak-points of the same person in subsequent trials. Hence, we keep the threshold as 20% of the database value. If the difference between total numbers of peaks for two FKP images goes beyond the threshold value, then those FKP images are considered to be of different people.

If the number of peak-points for input image matches with that of database, we proceed further. Now we have two sets of values containing peak-points – a set, *A* from the database for a particular person, and another set *B* is of input FKP image of a person waiting to get authenticated. The set *A* contains *M* number

of ordered pairs, each indicating a co -ordinate position of a peak point. Let us denote these ordered pairs as (x_{Ai}, y_{Ai}), where $i = 1 \ldots M$. Similarly, the set B contains N ordered pairs denoted by (x_{Bj}, y_{Bj}) where $j = 1 \ldots N$. Note that the sizes, M and N of two sets may not be same always. Even if the two sets A and B are derived from same person, due to possible noise and/or distortion during image acquisition, there is a chance of having different number of peak points. If N is not more/less than 20% of M, then only we proceed further. Now, compute the consecutive distance between the points in A as –

$$d_{Ai} = \left(x_{Ai} - \sqrt{x_{A(i+1)}}\right)^2 + \left(y_{Ai} - y_{A(i+1)}\right) \quad (10)$$

Here, $i = 1 \ldots M - 1$. Similarly, the successive distances between the points in B are –

$$d_{Bj} = \left(x_{Bj} - \sqrt{x_{B(j+1)}}\right)^2 + \left(y_{Bj} - y_{B(j+1)}\right)^2 \quad (11)$$

Here, $j = 1 \ldots N - 1$. Then we compare d_{Ai} and d_{Bi}. In case of non-equality among M and N, we compare only $min\ (M - 1, N - 1) = n$, say, distances. For any $i = 1 \ldots n$, if $d_{Ai} - d_{Bi} < 5.0$, we consider it as success, otherwise failure. The threshold value 5.0 is set to allow possible variation in the distances due to some noise during image acquisition.

After comparing the distances, we get a sequence of successes and failures. Now we compute the probability of success as –

$$P = \frac{\text{the number of success observed}}{\text{total number of comparisons made}} = \frac{S_{count}}{n} \quad (12)$$

The probability always ranges from 0 to 1 indicating no chance to 100% chance. If the computed value of P is greater than 0.60 (a threshold value), then the person can be accepted, otherwise he will be rejected. The algorithm for computation of probability is given in *Table II*.

TABLE II.
ALGORITHM FOR CALCULATING PROBABILITY OF SUCCESSFUL MATCHES BETWEEN PEAK POINTS

/* **Input:** Set A containing m ordered pairs $(x_{A1}, y_{A1}) \ldots (x_{Am}, y_{Am})$. And, set B containing n ordered pairs $(x_{B1}, y_{B1}) \ldots (x_{Bn}, y_{Bn})$.
Output: The probability P of successful matches between points in A and B.
*/
begin
Initialize $S_{Count} = 0$, $F_{Count} = 0$
if $abs(m - n) > 0.2 * m$ or $abs(m - n) > 0.2 * n$ then
$P = 0$
else
for $i = 1$ to m
$d_{Ai} = sqt\ [\ (x_{Ai} - x_{A(i+1)})^2 + (y_{Ai} - y_{A(i+1)})^2\ ]$
end for
for $j = 1$ to n
$d_{Bj} = sqrt\ [(x_{Bj} - x_{B(j+1)})^2 + (y_{Bj} - y_{B(j+1)})^2\ ]$
end for
for $i = 1$ to $min(m - 1, n - 1)$
if $(d_{Ai} - d_{Bi}) \leq 5.0$ then
$S_{Count} = S_{Count} + 1$
else
$F_{Count} = F_{Count} + 1$
end
if end
for
$P = \frac{S_{Count}}{\min(m-1, n-1)}$
end if
end

E.Iris Recognition

The proposed framework consists of three modules: image pre-processing, feature extraction, and recognition modules. Since the system is tested on the UBIRIS iris image database [8], this paper takes no account of the iris image acquisition module. The entire system flow is briefly described as follows. First, the iris image pre-processing module (IIP module) employs some image processing algorithms to demarcate the region of interest from the input image containing an eye. It performs three major tasks including iris localization, iris segmentation coordinate transform, and enhancement for the input iris image. Next, the feature extraction module (IFE module) applies with embedded zerotree wavelet coding methods on these features to generate the iris feature codes. Finally, the iris pattern recognition module (IPR module) employs a minimum distance classifier according to Hamming distance metric to recognize the iris pattern by comparing the iris code with the enrolled in the iris code database.

F. Pre-processing Module

Input image does contain not only useful information from iris zone but also useless data derived from the surrounding eye region. Before extracting the features of an iris, the input image must be pre-processed to localize, segment and enhance the region of interest. The system normalizes the iris region to overcome the problem of variation in camera-to-eye distance and pupil ¶s size variation derived from illumination. Furthermore, the brightness is not uniformly distributed due to non-uniform illumination; the system must be capable of removing the effect and further enhancing the iris image for the following feature extraction. Hence, the image pre-processing module is composed of three units: iris localization, iris segmentation with coordinate transform, and enhancement units, as shown in Fig. 4.

1) Iris Localization Unit

In this unit, we must determine the useful part (i.e., iris) from an input image at first. The iris is an annular region between the pupil and the sclera. The inner and outer boundaries of an iris can be treated as non-concentric circles approximately. In order to make the iris localization efficient, the system performs an operation of enhancing principal edges and blurring useless edges on the copied and down sample image instead of the original one. Following that, the system estimates the centre coordinates of the iris first.

Since the iris typically is darker than the Sclera and its gray level distribution has a small variance, the system uses Extended -Minima (EM) morphology operator [9]. EM transform is the regional minima of the H-minima transform. H -Minima transform suppresses all minima in the intensity image which depth is less than a scalar. Regional minima are connected component of pixels with the same intensity value which external boundary pixels all have a greater value than a scalar. We used 8-connected neighbourhoods in this process. By choosing an appropriate scalar in EM transform, a perfect edge of outer boundary is obtained. The value of threshold is decided, according to the histogram.

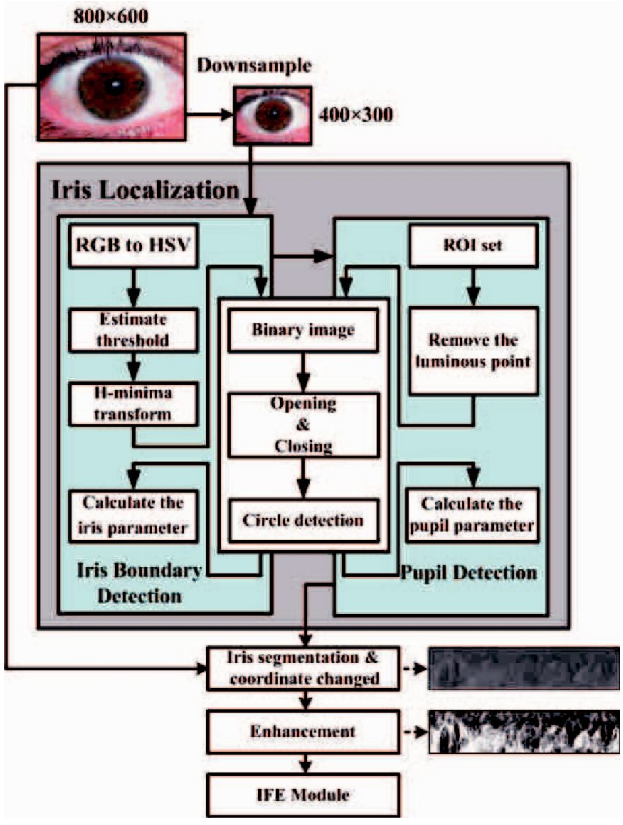

Fig. 4 Pre-processing module

2) Iris Segmentation and Coordinate Transform Unit

The localized iris zone demarcated from the human eye is transformed from rectangular into polar coordinate system so as to facilitate the following feature extraction module. When acquiring the human eye image, the iris zone images may be of different sizes (outer and inner boundaries of iris) due to the variations of camera-to-eye distance and/or environment ¶s illumination. The variations will change the patterns of iris texture to some extent. To solve this problem, it is necessary to compensate for the iris deformation. Daugman ¶s system uses radial scaling to compensate for overall size as well as a simple model of pupil variation based on linear stretching [2]. This scaling serves to map Cartesian image coordinates to dimensionless polar image coordinates. In addition, eyelids and eyelashes generally obscure the upper limbus of an iris, so the procedure needs to cut out the obscured area. The system generates a rectangular iris image of a fixed size by linear interpolation. The image size of iris is 512υ128.

3) Enhancement Unit

The normalized iris is easily affected by the non-uniform illumination and may have low contrast. The final step of the IIP module is to perform image enhancement in order to obtain a good-quality image, which presents clearer texture. The enhancement algorithm uses histogram equalization for the normalized iris image to compensate for the non-uniform illumination.

IV. IMPLEMENTATION AND PERFORMANCE ANALYSIS

The proposed technique is implemented using MatLab 7.5. The proposed algorithm is tested on FKP images taken from PolyU FKP Database. The PolyU FKP database provides original images as well as images of extracted region of interest. Simulation is done on FKP images of 165, including males and females, in the age group of 20 to 50. Most of the previous research works based on FKP focused on human identification but not authentication. Moreover, the previous approaches were computationally complex. In our algorithm, the problems in having mass storage of FKP image is overcome by storing the number of peaks and coordinate positions of those peaks in a Gabor Wavelet Image against UID.

Simulation results show that the False Acceptance Ratio (FAR) for the proposed algorithm is 1.24% and the False Rejection Ratio (FRR) is about 1.11%. We have tested our algorithm on varying thresholds for probability. The above results were obtained when the threshold was set for 0.60. The Receiver Operating Characteristic (ROC) curve obtained for the proposed system for varying threshold values is as shown in Figure 5.

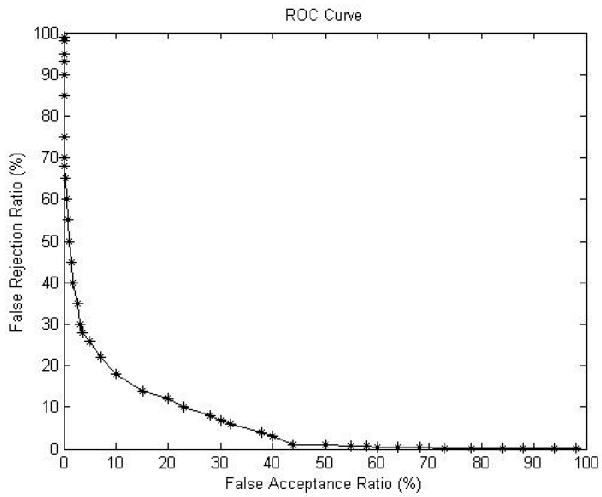

Fig. 5 ROC curve for Proposed Technique

V. CONCLUSION

In this paper, we propose an efficient way for human authentication using FKP images. In the proposed technique, we have applied LDA pre-processed FKP image. In IRIS proposed technique, we have applied is Gabor Wavelet transform on the pre-processed IRIS image. Then we plot a Gabor Wavelet graph and peak points are identified. The number of peak points and their locations are stored in the database.

To authenticate a person in question, we first compare the number of peak points in the Gabor Wavelet graph and that in database for a given UID. If they did not match for pre-set threshold value, the person can be rejected. Otherwise, the successive distances between the peaks are computed. Now, individual distances in the database and new image are compared. Every match for a given threshold is considered to be success count and a non-match as a failure. The probability of success is then computed. If the computed probability is greater than 0.60, the person can be accepted. Otherwise, he will be rejected.

The proposed technique is easily adaptable in real time situations as it is based on simple image processing techniques. The computational complexity found in previous works is reduced here. Suitable graphical user interface (GUI) can be developed to ease real time implementation. The proposed algorithm produces promising results with 1.24% of FAR and 1.11% of FRR.

REFERENCES

[1] Ajay Kumar and Ch. Ravikanth, “Personal authentication using finger knuckle surface”, *IEEE Trans Info. Forensics Security*, vol. 4, no. 1, pp. 98 – 110, March 2009.

[2] D. L. Woodard and P. J. Flynn, “Personal identification utilizing finger surface features”, *In Proc. of CVPR-2005*, pp. 1030 – 1036, 2005.

[3] Lin Zhang, Lei Zhang, David Zhang, and Hailong Zhu, “Online finger-knuckle-print verification for personal authentication”, *Pattern Recognition*, vol. 43, no. 7, pp. 2560 – 2571, July 2010.

[4] Lin Zhang, Lei Zhang, and David Zhang, “Finger-knuckle-print: A new biometric identifier”, *In Proc. of IEEE Int. Conf. on Image Processing*, 2009.

[5] Camus, T.A.; Wildes, R.; , "Reliable and fast eye finding in close-up images," Pattern Recognition, 2002. Proceedings. 16th International Conference on , vol.1, no., pp. 389- 394 vol.1, 2002.

[6] Yu Chen; Jin Wang; Changan Han; Lu Wang; Adjouadi, M.; , "A robust segmentation approach to iris recognition based on video," Applied Imagery Pattern Recognition Workshop, 2008. AIPR '08. 37th IEEE , vol., no., pp.1-8, 15-17 Oct. 2008.

[7] J. G. Daugman, “High Confidence Visual Recognition of Persons by a Test of Statistical Independence”, IEEE Transaction on Pattern Analysis and Machine Intelligence, vol. 15, no. 11, 1993, pp. 1148-1161.

[8] T. Camus and R. Wildes, "Reliable and Fast Eye Finding in Close-up Images", 16th International Conference on Pattern Recognition, vol. 1, 2002, pp. 389-394.

[9] Barzegar, N.; Moin, M.S.; , "A new approach for iris localization in iris recognition systems," Computer Systems and Applications, 2008. AICCSA 2008. IEEE/ACS International Conference on , vol., no., pp.516-523, March 31 2008-April 4 2008.

[10] Tianyi Zhang; Yongmei Hu; Chunxiao Zhang; Heng An; Wenwen Xu; , "A New Method for Iris' Location Based on Pointwise Detection," *Bioinformatics and Biomedical Engineering (iCBBE), 2010 4th International Conference on* , vol., no., pp.1-4, 18-20 June 2010.

[11] Belcher, C.; Yingzi Du; , "A Selective Feature Information Approach for Iris Image-Quality Measure," Information Forensics and Security, IEEE Transactions on , vol.3, no.3, pp.572-577, Sept. 2008.

[12] Kalka, N.D.; Jinyu Zuo; Schmid, N.A.; Cukic, B.; , "Estimating and Fusing Quality Factors for Iris Biometric Images," Systems, Man and Cybernetics, Part A: Systems and Humans, IEEE Transactions on , vol.40, no.3, pp.509-524, May 2010.

AUTHOR’S PROFILE

Author M.Bhavani is an M.Tech student in Computer science & engineering, Dr.MGR Educational and Research Institute University, Chennai, Tamil Nadu, India.